Hydrogen insertion in the intermetallic GdScGe: a drastic reduction of the dimensionality of the magnetic and transport properties

Tadhg Mahon, Etienne Gaudin, Antoine Villesuzanne, Rodolphe Decourt, Jean-Louis Bobet, Olivier Isnard, Bernard Chevalier, Sophie Tencé

Hydrogen insertion in the intermetallic GdScGe: A drastic reduction of the dimensionality of the magnetic and transport properties

Tadhg Mahon[†,‡], Etienne Gaudin[†,‡], Antoine Villesuzanne[†,‡], Rodolphe Decourt[†,‡], Jean-Louis Bobet[†,‡], Olivier Isnard[§], Bernard Chevalier[†,‡], Sophie Tencé [†,‡,*]

† CNRS, ICMCB, UMR 5026, F-33600 Pessac, France

‡ Univ. Bordeaux, ICMCB, UMR 5026, F-33600 Pessac, France

§ CNRS, Université Grenoble Alpes, Institut Néel, 38042 Grenoble, France

[*] Corresponding author. Tel.: +33 5 40006678; fax: +33 5 4000 2761

E-mail address: sophie.tence@icmcb.cnrs.fr (S. Tencé)

ABSTRACT

Intermetallic phases have been investigated with respect to their ability to accept small atoms in interstitial sites without changing the host structure. Among those, the intermetallic compounds crystallizing in the tetragonal CeScSi-type structure are able to absorb hydrogen atoms. These compounds are of particular interest because they can show electride-like character and, therefore, can be exploited as new catalysts. Here we report the case of GdScGe which uptakes hydrogen at 623 K and under a H_2 gas pressure between 0.5 to 4 MPa. The formation of the hydride GdScGeH, with H atoms entering into the [Gd_4] tetrahedra, preserves the host structure but induces an anisotropic volume expansion with a strong increase of the *c* parameter and a slight decrease of the *a* parameter. Interestingly, we show for the first time for this family of materials that hydrogen insertion reduces the dimensionality of the magnetic and transport properties from 3D to quasi-2D which results in a vanishing of the ferromagnetic order (T_C = 350 K for GdScGe) and a change of the metallic conduction behavior to a non-metallic one. As evidenced by density functional theory calculations, such drastic effects are accounted for through the Gd-H chemical bonding effect and the oxidizing effect of H whereas the volume expansion plays only a minor role.

Keywords: Rare-earth ternary compounds; CeScSi-type structure, Hydrogen; magnetic and transport properties, Density functional theory calculations

1. Introduction

The equiatomic *RTX* intermetallics (*R* = rare-earth, *T* = transition metal, *X* = p-block element) have been the subject of intensive investigations because of the large variety of structure types and physical properties encountered for this specific composition. Among these structures, one can cite the two tetragonal layered CeFeSi- and CeScSi-type structures that are both made of layers of [R_4] edge-sharing rare-earth tetrahedra alternating with layers made of *T* and *X* atoms. Such structures are of particular interest due to their ability to accept small atoms in the [R_4] tetrahedra which is also a way to reduce the dimensionality of the structure by pulling apart the two types of layers. In both structures the *T* atoms form a square net and are surrounded by four *R* and four *X* atoms leading to a coordination number equal to twelve. In the CeFeSi-type structure the *T* atoms are in the center of [R_4] and [X_4] tetrahedra whereas in CeScSi-type, they are located in [R_4] and [X_4] square planes. In both cases the coordination polyhedron for *T* atoms can be, in a first approximation, considered to be a cuboctahedron, strongly distorted in the case of CeFeSi-type structure.

In the CeFeSi-type compounds hydrogen insertion has been widely studied.[1] In all cases, hydrogen uptake results in the formation of hydrides with the composition *RTX*H, adopting the ZrCuSiAs-type structure like the 1111 iron-based superconductors.[2-5] The effect of hydrogenation on the magnetic properties can be very diverse, especially in the Ce compounds where RKKY (Ruderman-Kittel-Kasuya-Yoshida) and Kondo interactions are in competition. For example, the antiferromagnetic order in CeCoSi and CeCoGe vanishes in favor of a spin fluctuation behavior whereas the non-magnetic heavy-fermion CeRuSi becomes antiferromagnetic with a complex magnetic structure.[6,7] Another striking effect is the change of magnetic order type as in NdCoSi(Ge) which goes from an antiferromagnetic to a ferromagnetic one with a higher ordering temperature.[8] Also, in the case where both rare-earth and transition metal are magnetic like in NdMnSi, the Néel temperature of the Mn sublattice increases strongly while that of the Nd sublattice decreases.[9] Most interestingly, hydrogen insertion in the Pauli paramagnet LaFeSi leads to superconductivity with onset at 11 K.[10] LaFeSiH is thus the first iron-based superconductor with FeSi as conductive layer instead of pnictogen- or chalcogen-iron layer. These hydrides examples as well as all the 1111 iron-based superconductors illustrate the outstanding potential of the "filled" CeFeSi-type structure in which the [R_4] tetrahedra are filled with a small anion like H^-, O^{2-} or F^-.

Concerning the CeScSi-type materials, many of them exhibit unusually high magnetic ordering temperatures with respect to the concentration of rare earth elements present in the compounds, such as GdTiGe (T_C = 376 K), NdScSi (T_C = 171 K) or *R*ScGe (*R* = Ce, Pr, Nd,

Sm, Tb and Gd; T_{order} = 46-350 K).[11-18] In their recent work, Skorek *et al*. and Mishra *et al.*, describe how the magnetism in such compounds does not arise solely from RKKY interactions between the rare earth elements.[19-20] Rather, they show through *ab*-initio calculations that the presence of a slight spin polarization of the Ti/Sc 3d electrons plays an important role in the high magnetic ordering temperatures of these compounds. Insertion of hydrogen in CeScSi-type compounds has been studied, but less extensively than in the CeFeSi-type compounds, because hydrogenation systematically results in a drastic reduction of the magnetic ordering temperature. It is clearly the case for GdTiGe, NdScSi and CeScSi(Ge).[11,21,22] The insertion of hydrogen in GdTiGe (T_C = 376 K) forms the GdTiGeH hydride which (i) crystallizes in a filled tetragonal CeScSi-type structure where all the [Gd_4] tetrahedra are occupied by hydrogen and (ii) exhibits a paramagnetic behavior above 4 K. This drastic ferromagnetic $\rightarrow$ paramagnetic transition induced by hydrogenation was partly explained by the decrease of the number of conduction electrons at the Fermi level with the formation of the H^- anion; this number plays an essential role on the strength of the indirect RKKY interactions governing the magnetic properties of the rare earth based intermetallics. However, the reduction of the RKKY interactions is not sufficient to explain the modification of the magnetic properties since it has been shown that Ti polarization also plays a role. A similar effect is observed in NdScSi which shows a reduction of its Curie temperature from 171 K to 4 K upon hydrogenation and in CeScSi(Ge) with a decrease of T_N from 26 K (Si) and 43 K (Ge) to 3 K.[21,22] In all cases hydrogen uptake produces an anisotropic expansion of the unit cell with the *a* parameter decreasing and the *c* parameter strongly increasing. Yet, the amount of absorbed hydrogen can vary since GdTiGe and NdScSi compounds absorb 1 H f.u.$^{-1}$ and 1.5 H f.u.$^{-1}$ respectively. In this last case, hydrogen atoms occupy not only [Nd_4] tetrahedra but also [Sc_4Nd] pyramidal sites. Interestingly, the presence of these two sites is supposed to be connected to the electride-like character of the CeScSi-type compounds as evidenced in La_2Sb and LaScSi.[23,24] Electrides are compounds that contain excess electrons periodically located in crystallographic sites throughout the lattice. In LaScSi these electron anion are precisely located in the interstitial voids where the hydrogen atoms are inserted. Thus, electrides possess a strong electron-donating capacity that can notably be exploited for catalytic reactions. For example, the LaScSi silicide, when loaded with ruthenium, shows excellent catalytic activity for ammonia synthesis.[24] This is ascribed to the ability of LaScSi to both supply electrons to Ru and absorb reversibly hydrogen during the NH_3 synthesis, preventing H poisoning of the Ru surface. Therefore, CeScSi-type compounds present a high potential for heterogeneous catalysis, and more generally for the investigation of electride materials.

Among the *RTX* intermetallics crystallizing in the CeScSi-type structure the ternary germanide GdScGe displays a high Curie-temperature T_C, of close to 350 K,[14-16] *i.e.* higher than that of pure Gd metal. The high T_C of GdScGe suggested that this compound could exhibit an interesting magnetocaloric effect around room temperature but, finally, a moderate effect was determined, lower than that of pure Gd.[15] Another way to exploit the magnetic properties of the germanide was to perform chemical substitutions, such as Ge ↔ Sb, to induce competing magnetic interactions and structural instability.[25] The substitution of antimony for germanium leads to a gradual reduction of T_C, then to a structural change to a CeFeSi-type structure displaying an antiferromagnetic order at around 55 K.

In this context, we performed hydrogenation of GdScGe to complete the previous studies and unravel the question of hydrogenation's effect on the magnetic and electronic properties of CeScSi-type compounds. In particular, the influence of hydrogen on the magnetic behavior of the transition metal will be clarified for the first time. The second objective is to use hydrogenation to modify the transport properties of GdScGe as our previous study on CeScSi(Ge) has shown interesting change in resistivity behavior.[22] Here we present the results of this study, detailing the structural, magnetic and electronic transport properties of GdScGeH through powder X-ray diffraction, magnetization, resistivity and specific heat measurements. Based on density functional theory (DFT) calculations, these results are explained in term of the reduction of the dimensionality of magnetic and electronic properties. A similar conclusion was established about the hydrogenation of the CeFeSi-type compound CaNiGe,[26] but in our paper, we show that this effect can be even more pronounced in a CeScSi-type compound with the example of GdScGe.

2. Experimental

GdScGe and LaScGe samples used in the present study were prepared and characterized as described previously.[15,22] Hydrogen absorption experiments were performed using the apparatus formerly described.[27] The hydrogenation of LaScGe was carried out at 523 K and 4 MPa of H_2 as detailed previously.[22] The GdScGe ingots were heated under vacuum at 623 K for 2 h and then exposed to 4 MPa (sample 1) or 0.5 MPa (sample 2) of hydrogen gas at the same temperature. Under these experimental conditions, GdScGe ternary germanide absorbs hydrogen. The amount of absorbed H was determined volumetrically by monitoring pressure changes in a calibrated volume. The formed hydride is stable in air. Also, the H absorption induces decrepitation of the pure starting ingot into small grains.

X-ray powder diffraction data for the structural determination of GdScGeH hydride were collected at room temperature with a PANalytical X'pert PRO MPD diffractometer in Bragg-Brentano θ-2θ geometry with a Ge (111) monochromator and Cu-Kα1 radiation (λ = 1.5406 Å). The powder diffraction pattern was scanned over the angular range 10.0002°–130.0581° with a step size of Δ(2θ) = 0.0084°. Rietveld refinement was performed using the Jana2006 program package.[28] The background was adjusted manually and the peak shapes were described by a pseudo-voigt function. An absorption correction has been used to avoid negative value of the atomic displacement parameters (ADPs) induced by the very high absorption coefficient of the hydride and the huge amount of Gd. Analysis of the X-ray powder pattern for both samples shows that the hydride adopts a structure similar to the one of the parent ternary germanide GdScGe with the space group *I4/mmm.* The best Rietveld refinement has been obtained for sample 2 and was used to determined atomic positions and cell parameters. The refined unit cell parameters for GdScGeH are *a* =4.1595(3) and *c* =16.5017(12) Å. The reliability factors determined at the end of the refinement were R_p/R_{wp} = 1.90/2.45 % and $R_{F(obs)}/R_{B(obs)}$ = 5.86/10.06 %. The final atomic positions *x, y, z* and isotropic atomic displacement U_{iso} parameters are gathered in Table 1 and the interatomic distances in Table 2.

Table 1. Atomic coordinates† and isotropic atomic displacement parameters (Å^2) for the metal atoms in GdScGeH (space group *I*4/*mmm*, *a* = 4.1595(3) and *c* = 16.5017(12) Å).

Atom	Site	*x*	*y*	*z*	U_{iso} (Å^2)
Gd	4*e*	0	0	0.3153(2)	0.0095(11)
Sc	4*c*	0	1/2	0	0.009(3)
Ge	4*e*	0	0	0.1154(4)	0.011(2)

Table 2. Interatomic distances (Å) in the structures of GdScGe and GdScGeH

		GdScGe[15]	GdScGeH
Gd	4 Ge	3.108	3.156(3)
	1 Ge	3.054	3.299(7)

	4 Sc	3.480	3.690(3)
	4 Gd	3.768	3.646(3)
	4 Gd	4.253	4.1595(5)
	1 Gd	5.511	6.096(5)
	4 Gd	6.014	5.8825(5)
Sc	4 Ge	2.900	2.820(4)
	4 Sc	3.007	2.9412(3)
	4 Gd	3.480	3.690(3)
Ge	4 Sc	2.900	2.820(4)
	4 Gd	3.108	3.156(3)
	1 Gd	3.054	3.299(7)
	1 Ge	3.944	3.809(9)
H/Td[†]	4 Gd	2.411	2.342

[†]For the calculation of distances the (0, ½, ¼) atomic coordinates has been used for H or the empty Gd_4 tetrahedral site.

The physical characterizations will be mostly presented for sample 2 because GdScGeH is better crystallized than in sample 1 due to the use of milder conditions of hydrogenation (additional measurements for sample 1 are provided in Supporting Information). Magnetization measurements were performed using a superconducting quantum interference device (SQUID) magnetometer (Quantum Design MPMS-XL) in the temperature range 1.8–300 K and applied fields up to 7 T. For electrical resistivity measurements, the hydride powder was compacted at room temperature (compactness ≈ 80%) in order to form a polycrystalline pellet (diameter = 3 mm and thickness = 1 mm) and then heated for 2 days at 623 K under a pressure (0.5 MPa) of hydrogen. After this thermal treatment, which improves the mechanical behavior, the pellet was checked by X-ray diffraction; no structural change was evidenced. The measurement was carried out above 1.8 K using the standard dc four probe method with silver paint contacts and an intensity current of 5 mA. Because of the low compactness and the presence of microcracks in the pellet, the absolute value of ρ could not be determined accurately; for this reason, a normalized representation ρ(T)/ρ(290 K) is given. Finally, heat capacity measurements were performed on the same pellet using a standard relaxation method with a QD PPMS device. The sample of 25.1 mg was glued to the sample holder using Apiezon N-grease. The heat capacity of the sample holder and grease was measured just before the sample was studied.

Density functional theory (DFT) calculations were performed using the projector augmented-wave (PAW) method as implemented in the VASP code.[30-32] PAW datasets were used to describe valence electron-ionic core interactions, with valence Gd 4f, 5s, 5p, 6d, 6s, Sc

3p, 3d, 4s, Ge 3d, 4s, 4p and H 1s electrons treated explicitly. The exchange and correlation energies were treated at the generalized gradient approximation (GGA) level, according to the Perdew-Burke-Ernzerhof formulation;[33] an on-site Hubbard correction (*U*) of 5 eV was added to Gd 4f orbitals, according to Dudarev's scheme.[34] In a second set of calculations, we used the Heyd-Scuseria-Ernzerhof (HSE06) screened hybrid exchange functional, where 25% of GGA exchange is replaced by exact Hartree-Fock (HF) exchange.[35,36] The HSE06 scheme is much more demanding than GGA in terms of computational resources, but is expected to improve significantly the accuracy of calculated band gaps and crystal structures. Γ-centered Brillouin zone samplings of 16×16×4 and 8×8×2 *k*-points were used for GGA and HSE06 calculations, respectively.

3. Results and discussion

Hydrogen insertion

The hydrogenation curve of GdScGe (sample 2) is shown in Figure 1 along with the hydrogen absorption curve for the homologous phase GdTiGe previously studied.[11] The amount of H atoms inserted is 0.98(5) per GdScGe formula unit for sample 2. The result, around 1H f.u.$^{-1}$, was not determined with enough accuracy for sample 1 because of a slight leak in the apparatus at 4 MPa of H_2. In contrast to the recent study of the hydrogenation of the CeScSi-type compound NdScSi[21] both Gd*T*Ge (*T* = Sc or Ti) compounds absorb approximately 1 H f.u.$^{-1}$ The former compound was found to absorb 1.5 H f.u.$^{-1}$ with the hydrogen atoms distributed between two interstitial sites: [Nd_4] tetrahedral (1 H f.u.$^{-1}$) and [Sc_4Nd] square based pyramids (0.5 H f.u.$^{-1}$) leading to the overall formula $NdScSiH_{1.5}$. Therefore either hydrogen occupies only the [Gd_4] tetrahedral sites or both interstitial sites are partially occupied. It is noteworthy that the ScO impurity plays the role of activator/catalyst for hydrogenation: without ScO, the complete hydrogenation is virtually impossible, even if much higher H_2 pressure and operating temperature are used. This difficulty to hydrogenate has been systematically observed when a Sc metal reagent free of scandium oxide was used. The interest of transition metal oxides as catalysts for improvement of hydrogen sorption is well known.[37] Surprisingly, this effect was not observed during hydrogen insertion in the homologous phase GdTiGe, which can be achieved at mild conditions (figure 1) although no oxide is observed on XRD measurements.

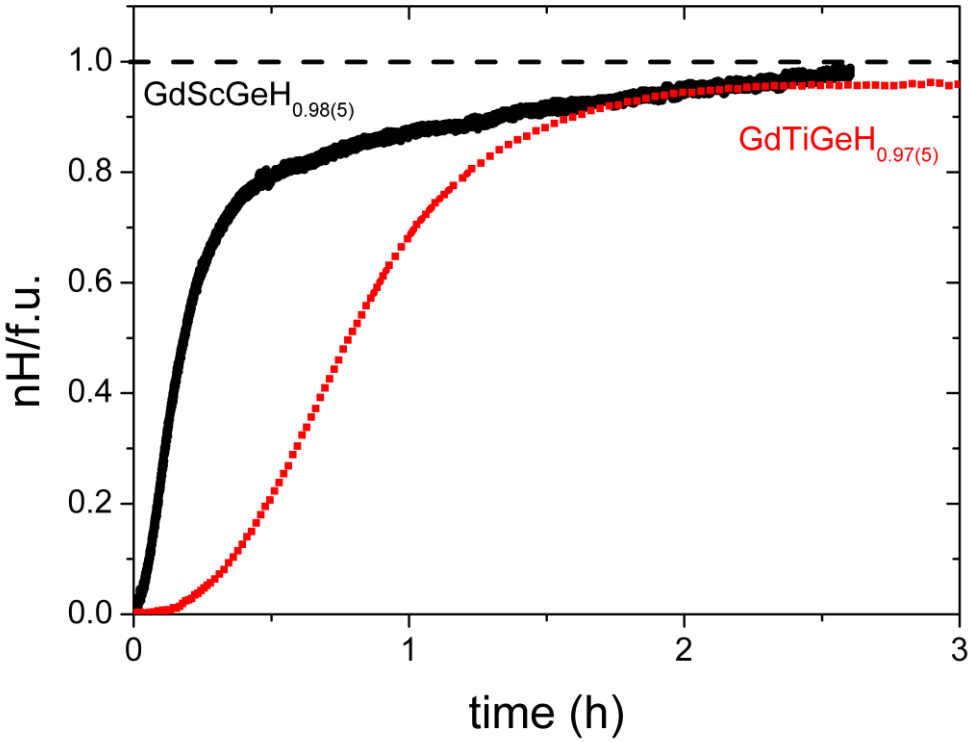

Figure 1. Hydrogen absorption curves of GdScGe (sample 2) and GdTiGe at 623 K and 0.5 MPa of H_2 gas.

Structural characterization

For sample 2 the impurity phase $ScO_{0.95}$ and the pristine GdScGe,[29] were taken into account for the Rietveld refinement of the X-ray diffraction data with a determined amount equal to 7.3 and 2.9 wt% respectively (for sample 1 see figure S1 in Supporting Information). Small extra broad peaks observed below 30° and at 35° correspond to an unknown impurity phase (marked with asterisks) which could be a decomposition product. Because of the medium quality of the diffraction pattern due to the strong absorption and fluorescence of Gd, the exact composition of the hydride was not determined (a full occupancy of all atomic positions was considered). From previous structural determination of the pristine sample on single-crystal it has been shown that its exact composition is $Gd_{1.02}Sc_{0.98}Ge$.[14,15] A slight deviation from ideal composition 1:1:1 and the certainly overestimated amount of Sc versus the Gd-based phase (despite the use of absorption correction) may explain the significant amount of ScO observed. Because of the low electron density of hydrogen it was not possible to refine or check its atomic position. The filling of the Gd_4 tetrahedra by H atoms has been assumed after the pressure change during hydrogenation and has been confirmed by band structure calculation (see below).

Thus, for the calculation of distances the (0, ½, ¼) atomic coordinates has been considered for H atoms (Table 2).

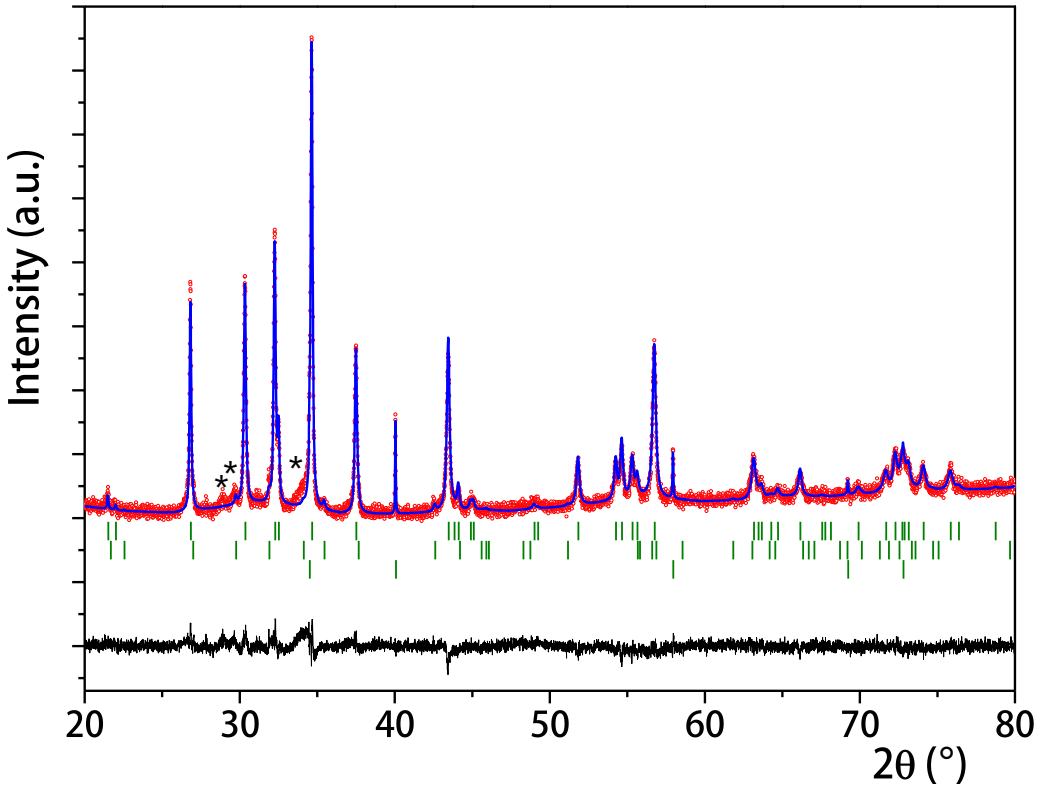

Figure 2. Rietveld refinement of GdScGeH (sample 2) XRD powder pattern measured with Cu-Kα_1 radiation (λ = 1.54051 Å) at T = 293 K (observed (cross), calculated (full line), and difference (bottom) profiles). The Bragg peak positions are indicated by tick marks for the main phase GdScGeH (upper row), the pristine phase GdScGe (intermediate row) and the impurity phase $ScO_{0.95}$ (lower row).

GdScGe crystalizes in the CeScSi-type structure which is an ordered derivative of the La_2Sb-type. This structure is made of two types of layers alternatively stacked along the *c*-axis. One consists of an infinite layer of edge-sharing, empty, Gd_4 tetrahedra and the other one of a square net of Sc-atoms located in the center of Ge_4 square planes (Figure 3).

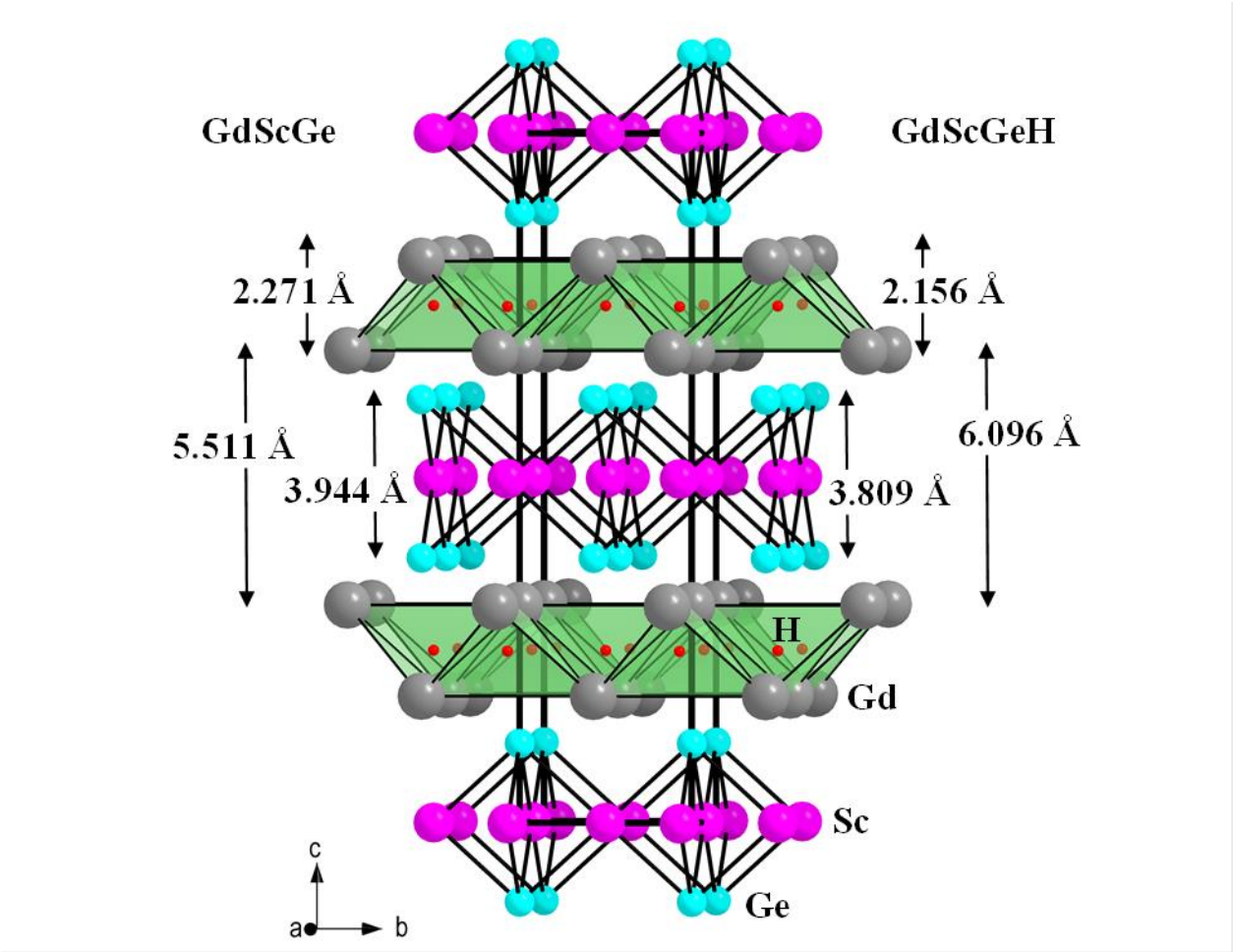

Figure 3. Crystal structure of GdScGeH where green edge-shared [Gd_4] tetrahedra and black Sc-Ge bonds are drawn. On the left (right) part of the figure selected distances for GdScGe (GdScGeH) are given.

Hydrogenation has a drastic anisotropic effect on the evolution of the unit cell parameters. The *a* parameter becomes smaller (from 4.2527(6) to 4.1595(3) Å) while *c* increases strongly (from 15.563(3) to 16.5017(12) Å), this induces an expansion of the unit cell volume from 281.5 to 285.5 $Å^3$ and a strong increase of the *c/a* ratio (from 3.66 to 3.97). Similar behaviour is reported after hydrogenation of the ternary compounds crystallizing in the CeScSi and CeFeSi-types which is linked to the filling of the [R_4] tetrahedral units by hydrogen.[1,22] The H-insertion into GdScGe also affects the atomic position of the Ge-atom: *z*(Ge) varies from 0.127 to 0.115 (Table 1);[15] the shifting of the Ge-atom along the *c*-axis causes a decrease of the Sc-Ge distance (Table 2). In the same way, *z*(Gd) decreases from 0.323 to 0.315 and the Gd-Gd distances in the Gd layer decrease. The hydrogenation has induced a shrinking of the two

different layers and an increase of the distance between them. This latter effect can be observed through the increase of the distance between Gd atoms located in successive layers of tetrahedra (from 5.51 to 6.10 Å, see Figure 3), this distance increases more, relatively, than the *c*-axis (+10.5% compared to +6.0 % for *c*). This behaviour suggests that the dimensionality of the crystal structure is reduced by hydrogenation of GdScGe. In Table 2 the H insertion into [Gd_4] tetrahedra has been considered for distance calculation (Table 2). One can notice that de Gd-H distance of 2.342 Å is very close to the one observed in GdH_2, 2.296 Å, with H in the same environment.[38]

Physical characterization

The temperature dependence of the reciprocal magnetic susceptibility χ_m^{-1} of GdScGeH measured with a magnetic field of 2 T is plotted in the inset of Figure 4 for sample 1. Above 50 K, the χ_m^{-1} *vs.* T curve is fitted with a Curie–Weiss expression $\chi_m^{-1} = (T-\theta_p)/C_m$ where C_m is the molar Curie constant and θ_p the paramagnetic Curie temperature. The estimated effective moment $\mu_{eff} = (8C_m)^{1/2}$ is found to be 7.84 μ_B, a value very close to that of the free-ion moment of the Gd^{3+} ion (7.94 μ_B). The θ_p value equal to 3.5 K is weakly positive, evidencing mainly ferromagnetic exchange interactions. The measurement for sample 2 leads to the same μ_{eff} value but the χ_m^{-1} curve is linear only above 250 K because of the presence of a small amount of residual ferromagnetic pristine GdScGe (see Figure 2).

The magnetization divided by the magnetic field M/H is depicted in Figure 4 for sample 2 and for fields of 0.02, 0.05 and 0.5 T after Zero-Field-Cooling (ZFC) and Field-Cooling (FC) process (see Figure S2 for sample 1). These magnetic measurements clearly unveil drastic modifications in comparison with the pristine compound GdScGe which undergoes a ferromagnetic transition at 350 K.[15] Indeed, the curves at the lowest fields show a maximum at 6 K which transforms into a kink for an applied field of 0.5 T. This indicates the presence of a magnetic transition at this temperature, below which the ZFC and FC curves slightly deviate from each other. This behavior may indicate the occurrence of an antiferromagnetic, canted ferromagnetic or ferrimagnetic ordering. The magnetization *vs.* field curves (M(H)) at 30 and 1.8 K are shown in Figure 5. A small spontaneous magnetization is still visible on the curve at 30 K, arising from the ferromagnetic signal of the residual pristine GdScGe still present in small quantity after hydrogenation. The non-linear behavior of M(H) at 1.8 K excludes a simple antiferromagnetic order. The application of increasing field seems to gradually change the initial state into a ferromagnetic one. Furthermore, the magnetization value at 7 T is close to 7

μ_B f.u.$^{-1}$ evidencing that the material is close to saturation (μ_{Gd3+} = 7.0 μ_B). This behavior is similar to that of Gd_5Si_3, for example, which is believed to be helimagnetic.[39] All these measurements suggest that GdScGeH has a complex magnetic behavior as often observed in magnetic CeScSi-type compounds.[40,41]

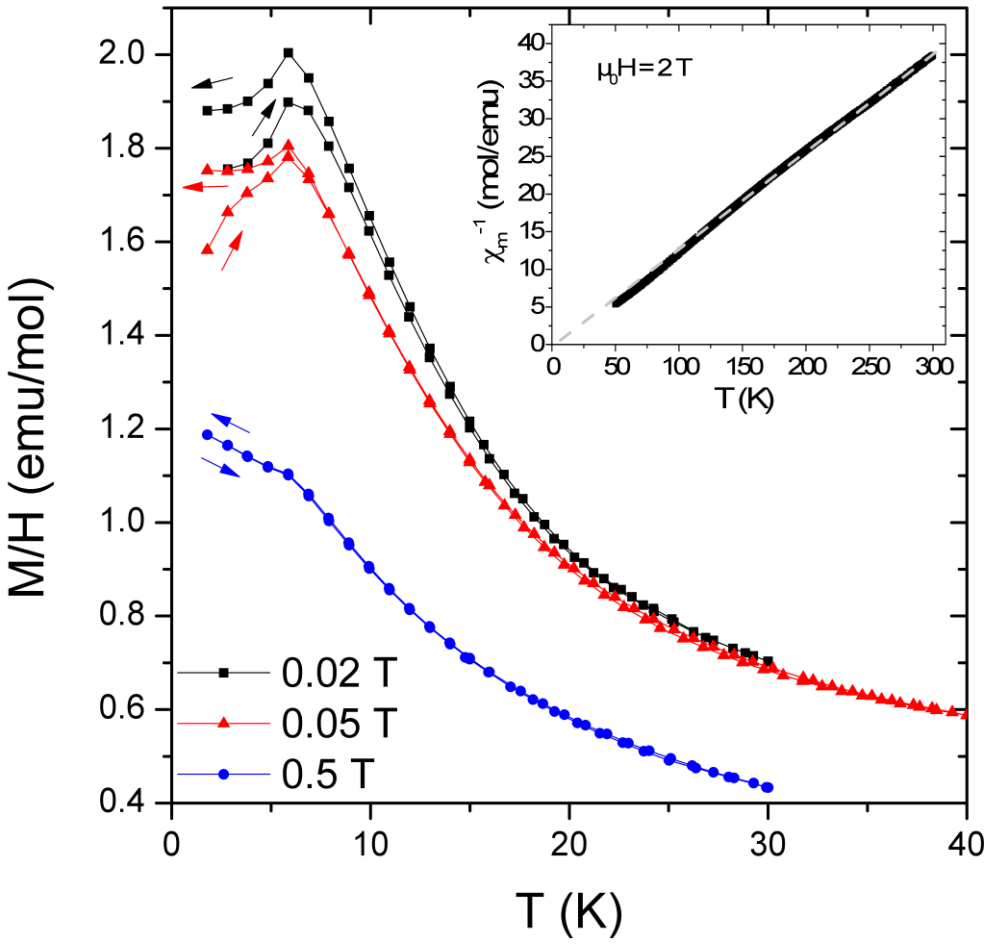

Figure 4. Temperature dependence of the magnetization M of GdScGeH divided by the applied magnetic fields H. ZFC and FC processes are indicated by arrows towards higher and lower temperatures, respectively. Inset: Temperature dependence of the reciprocal magnetic susceptibility χ_m^{-1} for the GdScGeH hydride (sample 1). The dashed black line shows the Curie-Weiss law.

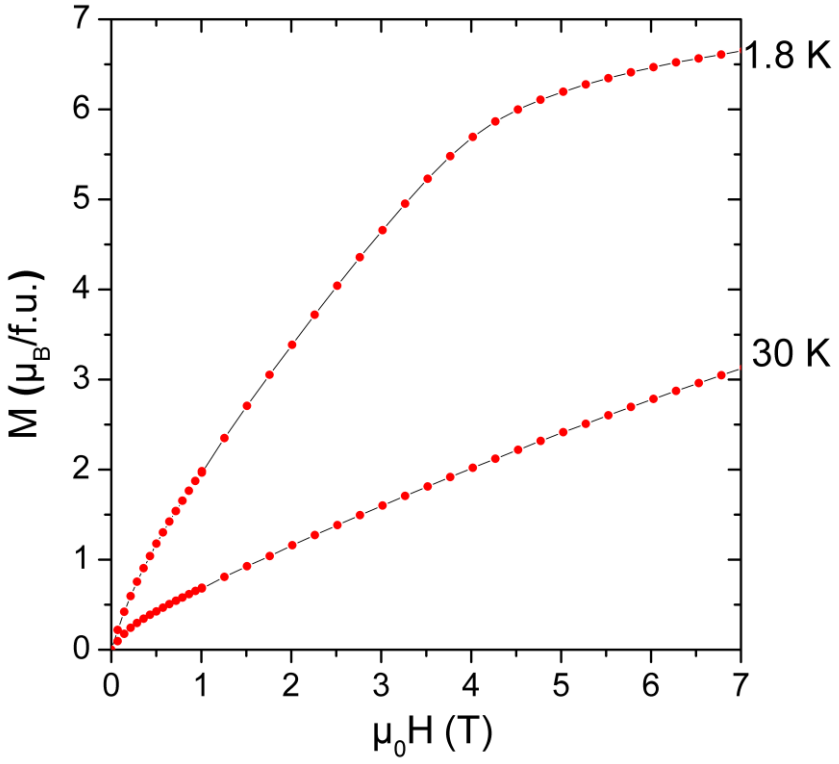

Figure 5. Isothermal magnetization curves of GdScGeH at 1.8 and 30 K.

The results of the specific heat, C_p, investigations for GdScGeH (sample 2) are presented in Figure 6. The temperature dependence of the specific heat measured in zero magnetic field discloses a sharp λ-peak at 6 K, evidencing the magnetic transition (Figure 6b). This observation corroborates very well the magnetization measurements. In order to accurately extract the magnetic contribution ($C_m(T)$) from the total specific heat using the formula $C_p = C_{el} + C_{ph} + C_m$, with C_{el} and C_{ph} the electronic and the phonon contributions, we first evaluated $C_{el}(T)$ and $C_{ph}(T)$. To evaluate these two contributions we measured the specific heat of the nonmagnetic isotype compound LaScGeH, assuming that $C_{el}(T)$ and $C_{ph}(T)$ are very close for both compounds. At low temperature, $C_{el}(T) + C_{ph}(T) = \gamma T + \beta T^3$ with γ the Sommerfeld coefficient and $\beta = 12\pi^4 nR/(5\theta_D^3)$ where n = number of atoms per formula unit, R = gas constant and θ_D the Debye temperature. By plotting Cp/T vs T^2 for LaScGeH (inset of Figure 6b), we observe a linear variation of the curve whose fit between 2 and 11 K gives $\gamma = 4.9$ mJ mol^{-1} K^{-2} and $\beta = 8.010 \times 10^{-4}$ J mol^{-1} K^{-4}. The β value corresponds to a Debye temperature θ_D of 273 K. We consider a similar electronic coefficient, γ, and Debye temperature for GdScGeH, even if we can expect a slightly smaller θ_D due to a small mass difference between both compounds. Note

that this mass correction was not performed in this data treatment. The magnetic contribution $C_m(T)$ of the Gd hydride was then determined by subtracting the electronic and the lattice contributions to the total specific heat, *i.e.* by subtracting the C_p curve of LaScGeH from that of GdScGeH. We obtain the magnetic entropy $S_m(T)$ by integrating $C_m(T)/T$ between 0 and T as plotted in insert of Figure 6a. It is shown that $S_m(T)$ reaches 12.5 J mol^{-1} K^{-1} at the ordering temperature, *i.e.* 72% of the theoretical maximum value, $Rln(2J+1)$ = 17.3 J mol^{-1} K^{-1}, for J = 7/2, value which is almost reached at around 30 K. Thus, this means that the total spin of Gd ion in the ground state of GdScGeH is 7/2.

(a)

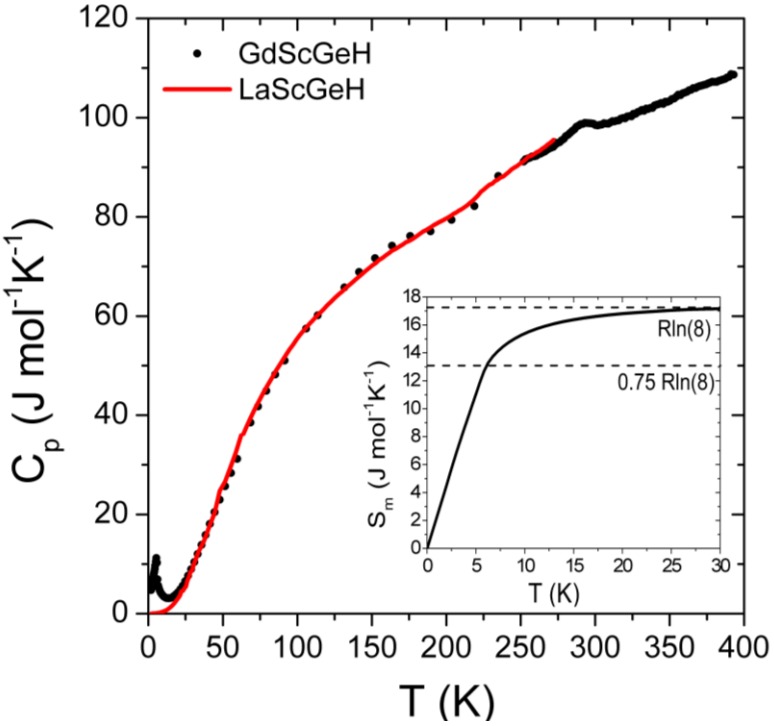

(b)

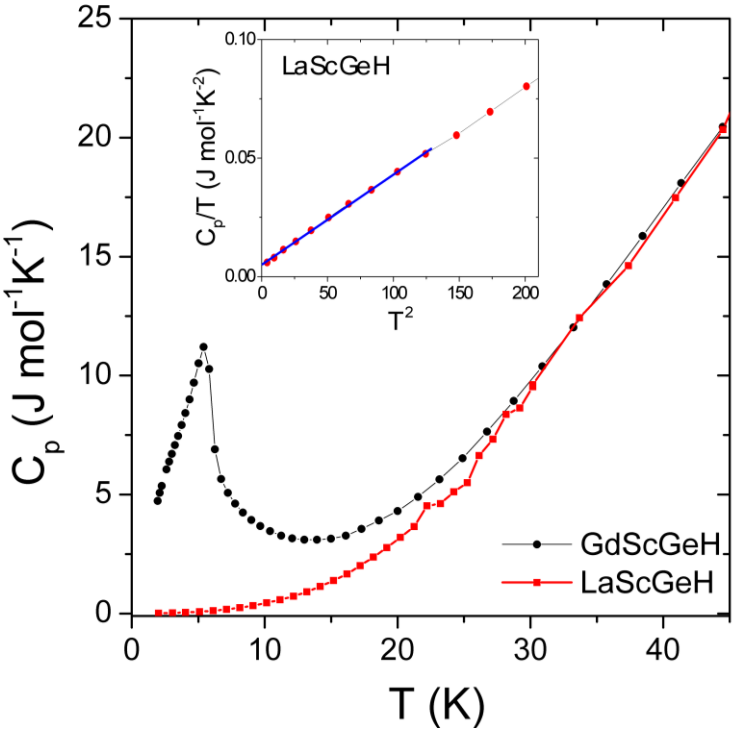

Figure 6. a) Temperature dependence of the specific heat of GdScGeH and the nonmagnetic isotype LaScGeH. The inset shows the temperature evolution of the magnetic entropy S_m with the positions of the theoretical maximum value Rln8 for J = 7/2 and of the S_m value at the magnetic transition. b) Zoom of the specific heat between 1.8 and 50 K for both compounds. The inset shows the plot of Cp/T vs T^2 for LaScGeH fitted with a linear law.

The temperature dependence of the normalized resistivities ρ/ρ_{290K} of GdScGe and GdScGeH hydride is depicted in Figure 7 (see Figure S3 for sample 1). Due to the low compactness of the pellets, *i.e.* around 80% only, we report the normalized resistivity curves. It is worth noting that the measured resistivity of the pellets is of the order of 10^{-3} Ω.cm for the pristine ($10^{-4}/10^{-5}$ Ω.cm for GdScGe in block form) and 10^{-2} Ω.cm for the hydride. Thus, the values for the pellets can be considered as an upper limit of the intrinsic resistivity of the compounds. The pristine compound shows a metallic behavior with $\partial\rho/\partial T > 0$ in the whole temperature range whereas the hydride exhibits a non-metallic behavior ($\partial\rho/\partial T < 0$) with an increase of the resistivity at low temperature. As visible in Figure S3, this enhancement of the resistivity at low temperature is stronger for sample 1 than for sample 2. Thus, hydrogenation induces a transition from metallic to non-metallic behavior. It is noteworthy that a similar effect of insertion of a small amount of hydrogen was also observed for the isostructural compounds LaScSi, CeSc(Si,Ge),[22] as well as for CeNiZn with the ZrNiAl-type structure.[42] For compounds with higher amounts of inserted hydrogen atoms, the effect can be more pronounced with the occurrence of metal-semiconductor-insulator transitions, as for example in the R_3Ni intermetallics with 8 H f.u.$^{-1}$.[43]

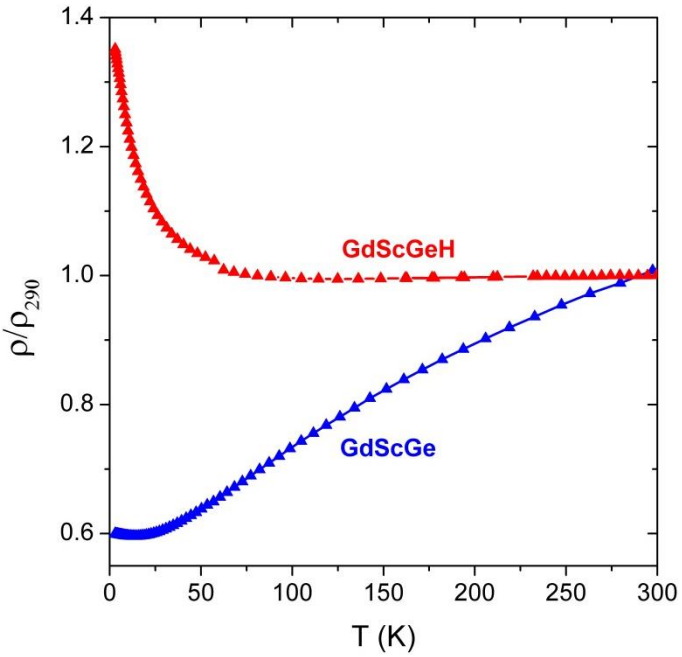

Figure 7. Temperature dependence of the normalized resistivity ρ/ρ_{290K} of the pristine compound GdScGe and GdScGeH formed under 0.5 MPa of H_2.

DFT calculations

Starting from experimental data, the atomic positions and lattice parameters were relaxed under space group *I4/mmm*, until the residual forces were less than 0.1 eV/Å. As shown in Table 3 and 4, the relaxed structural parameters are in good agreement with experimental values; the discrepancy is less than 1% for most values. HSE06 calculations are actually more accurate than GGA+*U* for the cell parameters. Surprisingly, however, GGA+*U* gives better results than the hybrid scheme for the *z* coordinate of Gd and Ge (4*e* site). Overall, the agreement between calculated and experimental crystal structures of GdScGe and GdScGeH is very satisfactory.

Table 3. Crystal structure for GdScGe and GdScGeH, calculated from DFT within the GGA+*U* and HSE06 schemes: unit cell parameters (constrained space group *I*4/*mmm*).

	a (Å)			*c* (Å)		
	GGA+*U*	HSE06	Exp.	GGA+*U*	HSE06	Exp.
GdScGe	4.2274	4.2445	4.2527(6)	15.6566	15.6283	15.563(3)
GdScGeH	4.1329	4.1648	4.192(2)	16.3525	16.3414	16.740(8)

Table 4. Crystal structure for GdScGe and GdScGeH, calculated from DFT within the GGA+*U* and HSE06 schemes: Gd and Ge atomic coordinates (4*e* position: *0 0 z*).

	z (Gd)			*z* (Ge)		
	GGA+*U*	HSE06	Exp.	GGA+*U*	HSE06	Exp.
GdScGe	0.3226	0.3226	0.32296(2)	0.1260	0.1243	0.12671(6)
GdScGeH	0.3164	0.3180	0.3155(5)	0.1169	0.1145	0.1162(7)

Table 5. Unit cell parameters for GdScGeH (S.G. *I*4/*mmm*, Z = 4), calculated from DFT within the GGA+*U* and HSE06 schemes, for two repartitions of the hydrogen atoms in [Gd_4] tetrahedral and [Sc_4Gd] pyramidal sites.

	a (Å)			*c* (Å)		
Hydrogen sites	GGA+*U*	HSE06	Exp.	GGA+*U*	HSE06	Exp.
4×[Gd_4]	4.1329	4.1648	4.192(2)	16.3525	16.3414	16.740(8)
2×[Gd_4] + 2×[Sc_4Gd]	4.1719	4.1926	4.192(2)	16.0540	15.6946	16.740(8)

In particular, GGA+*U* and HSE06 – with a better accuracy for the latter - allow the evolutions of *a* and *c* parameters during hydrogen insertion to be retrieved, *i.e.* the decrease of the *a* value vs. the significant increase in the *c* value. A better agreement between experimental and HSE06 values might be obtained for the structural parameters of GdScGeH, using a denser *k*-point grid, optimizing the percentage of HF exchange, and/or using a more severe convergence criterion for the residual forces; however, the expected improvement is not worth the (huge) corresponding computational cost, and we chose to rely on the satisfactory values readily obtained.

Note that we chose to place the hydrogen atoms in the [Gd_4] tetrahedral sites only. Calculations with hydrogen in both [Gd_4] and [Sc_4Gd] pyramidal sites led to a significantly worse agreement with the observed evolution of the *c* parameter during hydrogen insertion, knowing that hydrogenation essentially impacts the *c* parameter (Table 5). In $NdScSiH_{1.5}$, hydrogen atoms occupy both sites; however, GGA+*U* calculations (to be published) show that the [Sc_4Nd] pyramidal sites are favored by c.a. 370 meV/f.u. compared to [Nd_4] tetrahedral sites for hydrogen insertion in NdScSi. This is not the case in GdScGe, where the energy difference between the two sites does not exceed 75 meV/f.u.; this could explain why the hydrogen insertion rate does not go beyond GdScGeH in this compound.

Figure 8 shows the total density of states (DOS) for GdScGe and GdScGeH, calculated with the HSE06 functional and the relaxed crystal structures. GdScGe appears to be a half-metal ferromagnet, whereas a pseudo-gap or strong depletion of DOS at the Fermi level (E_F) was found for GdScGeH. The electron density in the range from E_F-0.1 eV to E_F is plotted in Figure 9. Features from both the DOS and electron density near E_F are consistent with the observation of a metallic character in the transport properties of GdScGe (Figure 7) and of a non-metal conduction in GdScGeH. From the point of view of our HSE06 calculations, GdScGe is a half-metal ferromagnet, with 3D electron conduction, whereas GdScGeH is no longer a band-like metal due to the pseudo-gap and 2D electron density distribution at E_F. Indeed, our results on the hydride indicate possible low-dimensional electron conduction and an anisotropic

conductivity is expected, i.e. when measured along the *c*-axis vs. in the (*ab*) plane. At this stage though, our DFT calculations do not give information about charge carriers' mobility.

The rather high resistivity and its weak dependence with temperature (Figure 7) indicate that GdScGeH is a clearly less metallic than GdScGe. However, the variation of $\rho(T)$ is too small to reflect a semiconducting behavior and no band gap E_g can be extracted from this curve, as expected from the non-zero density of state at E_F. It is difficult to discuss about the origin of the increase of resistivity at low temperature because the measurements are performed on pressed pellet and thus electron scattering on grain boundaries and weak contact between particles hamper the results interpretation. At this stage of the investigations, we can only mention some possible explanations: Kondo effect is unlikely since a similar behavior is also observed on the La isotype compound (no f electron). Besides, if magnetic impurities are present and induce Kondo effect this effect should be also seen in the pristine compound GdScGe since hydrogenation step does not bring extra magnetic impurities. In fact, the increase of the electrical resistivity can be explained by either a decrease of the conduction electrons density or by the localization of the conduction electrons. In GdScGeH, considering that the energy states at E_F are localized in a pseudo-gap, it is possible that the thermal activation of the conduction carrier gives rise to an increase of ρ at low temperature. The increase of resistivity at low temperature may also results from weak localization effect induced by disorder (Gd/Sc mixture, H vacancies or stacking faults). This would explain why the increase of resistivity with decreasing temperature is more pronounced in sample 1 (Figure S3) as GdScGeH is less well crystallized in sample 1 than in sample 2. Indeed, enlargement of the Bragg peaks indicate more structural defects due to use of higher H_2 gas pressure during hydrogenation, suggesting more strain in grains or possible small deviation of the amount of hydrogen from 1 H f.u.$^{-1}$ (within the limit of accuracy of the absorption experiment results). Further resistivity measurements under magnetic field would be useful to check this assumption as magnetic field is expected to reduce weak localization effect.

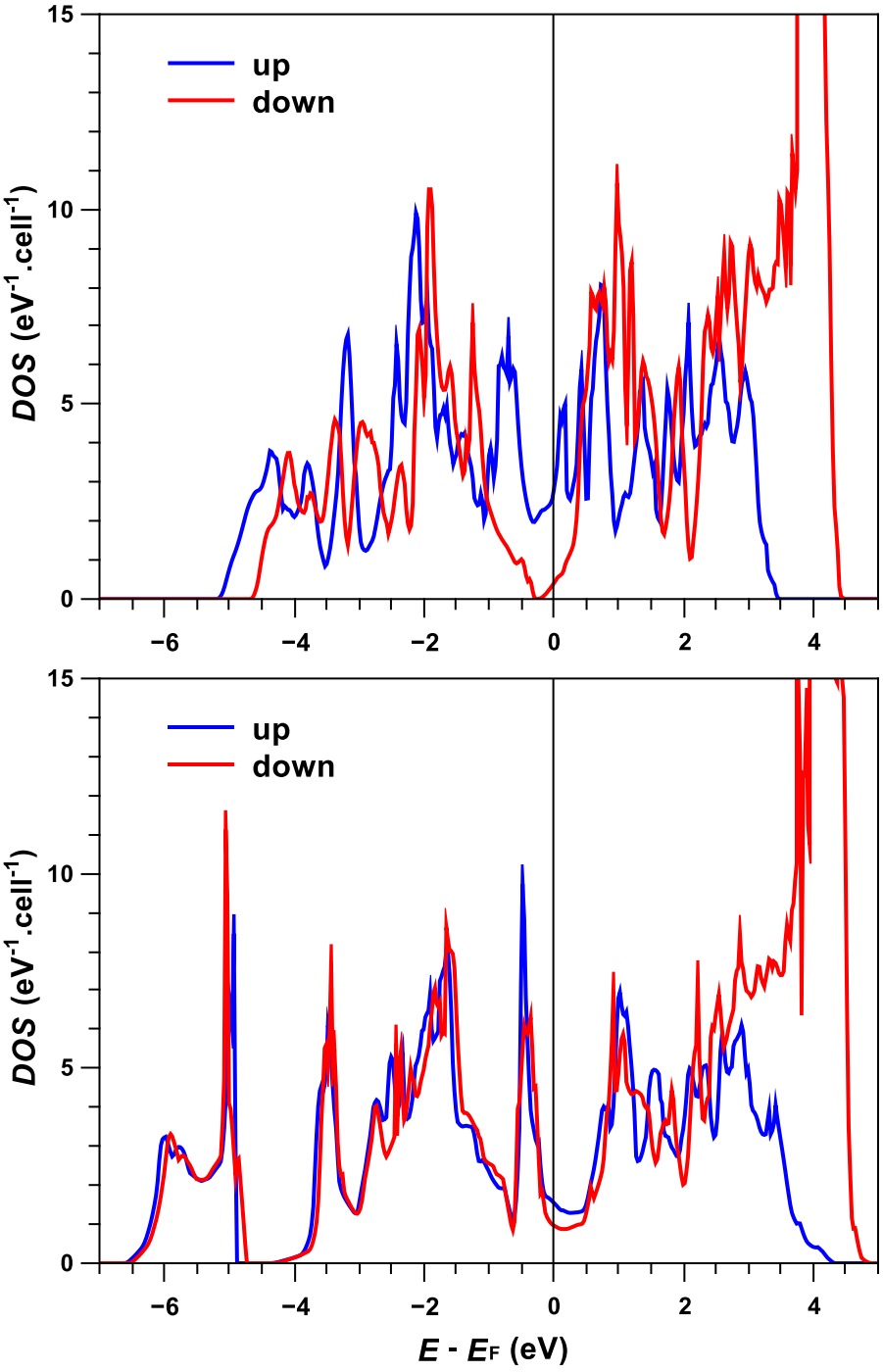

Figure 8. Density of states (DOS) for GdScGe (top) and GdScGeH (bottom), from spin-polarized DFT/HSE06 hybrid calculations. Majority and minority spin channels are indicated as up (blue) and down (red) lines, respectively.

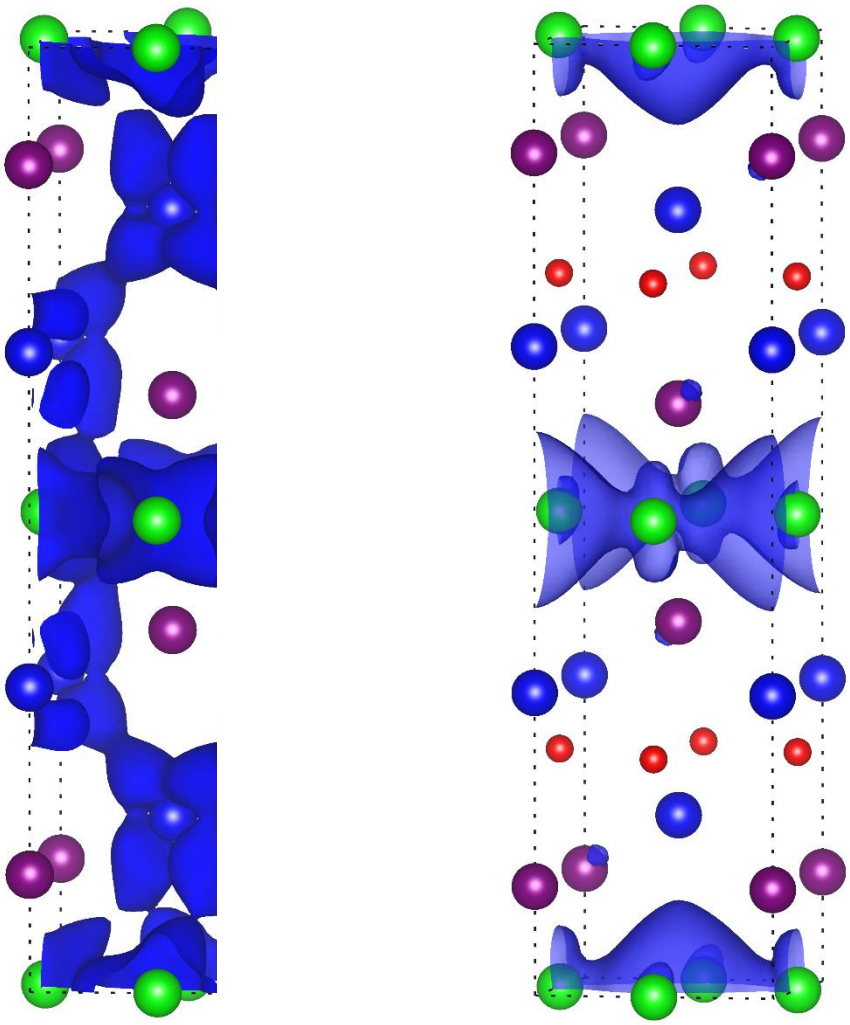

Figure 9. Isovalue plots of the electron density within a 0.1 eV range below Fermi level, for GdScGe (left) and GdScGeH (right), from DFT/HSE06 hybrid calculations. Blue, green, purple and red spheres represent Gd, Sc, Ge and H atoms, respectively. Plots were made using the software VESTA.

Another striking feature in Figure 10 is the disappearance of spin-polarization for GdScGeH, except for Gd 4f bands, when compared to the GdScGe DOS. Unpaired spin populations (listed in Table S1) confirm this trend, with vanishing contributions from Sc and Gd d orbitals/bands on hydrogen insertion. In GdScGe, the spin-polarization of the valence bands induces a magnetic moment in Sc 3d and Gd 4d/5d orbitals (0.22 and 0.40 μ_B, respectively), alongside a significant interaction between Sc $3d_{xz/yz}$ and Gd d orbitals; this is clearly seen in the spin density map shown in Figure 10. Sc $3d_{xz/yz}$ provide a magnetic path that couples the moments between Gd layers, along the *c* axis, and explains why GdScGe is ferromagnetic with a Curie temperature as high as 350 K. In GdScGeH, the spin polarization of the valence bands vanishes,

and the Gd-Sc magnetic paths as well; the 3D long-range magnetic order is almost lost, as observed experimentally, with a paramagnetic state from high temperature down to 6 K. Note that our results agree with densities of states and magnetic moments from DFT calculations, found in literature, for GdScGe.[19,40,44] No electronic structure investigation was made so far for GdScGeH, to our knowledge.

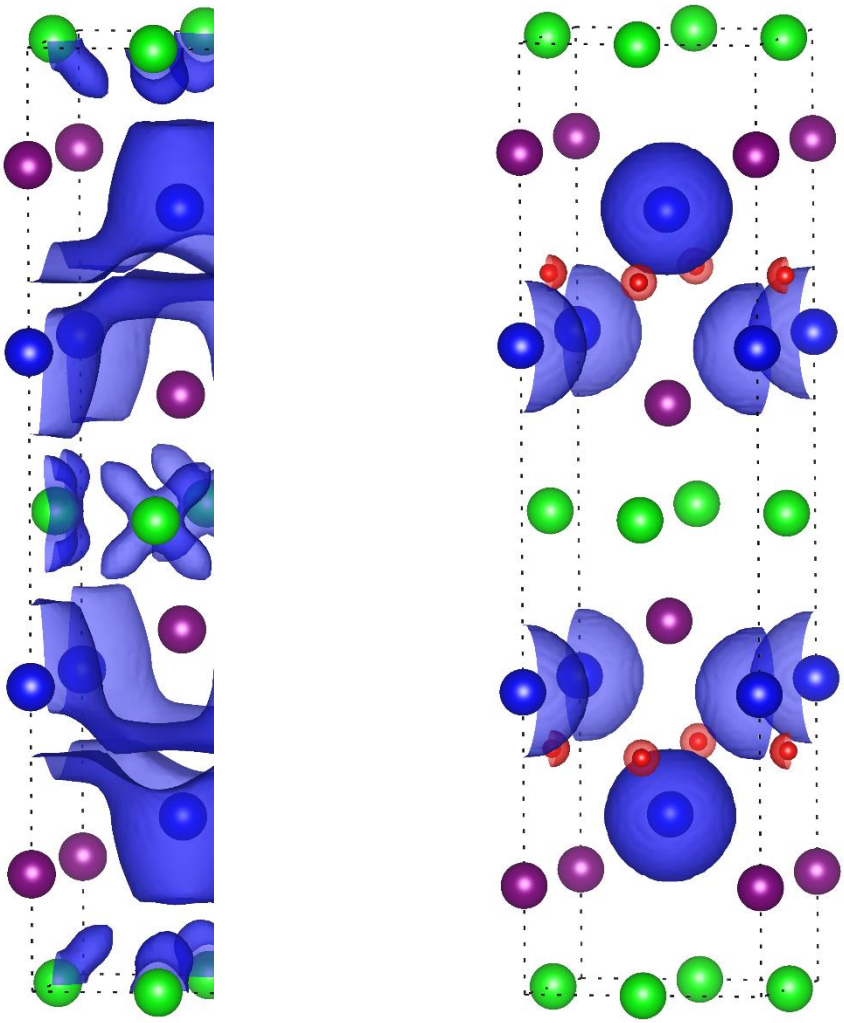

Figure 10. Isovalue plots of the unpaired spin density for GdScGe (left) and GdScGeH (right), from DFT/HSE06 hybrid calculations. Blue, green, purple and red spheres represent Gd, Sc, Ge and H atoms, respectively. Plots were made using the software VESTA.

A key question here is the way hydrogen insertion drives the disappearance of magnetism in the valence bands: is it indirectly, by i) significantly changing the crystal structure (if not the space group), *i.e.* bond lengths, ii) by its oxidizing effect (as seen in Figure 11, the hydrogen 1s band lies below the valence bands and hydrogen is unambiguously in the H^- state), or iii) by a

direct chemical bonding effect (Gd-H interactions competing with Gd-Sc interactions, via Gd d orbitals)? DFT calculations allow us to decorrelate those effects, by fixing the crystal structure to the chosen one, removing electrons (1 electron per formula unit, with a compensating background charge), and/or explicitly inserting hydrogen in the lattice (while keeping the lattice and/or the Fermi level fixed). We performed GGA+*U* calculations on all combinations (see Figures S4 and S5) and could conclude that both Gd-H bonding and charge transfer from the host lattice to hydrogen contribute to cancel the spin polarization in the valence bands. Importantly, calculations show that the changes in crystal structure, although significant, have no role in the loss of magnetism. The charge transfer depopulates the top of the valence band (which is of Sc and Gd d-character) thus decreasing both the population of these orbitals and the exchange stabilization of majority-spin bands. The Gd-H bonding interactions diminish Gd-Sc interactions through their respective d orbitals, thus also decreasing both the spin-polarization of Sc 3d orbitals and their role as a magnetic bridge or path for the magnetic coupling of Gd double layers along the *c* axis.

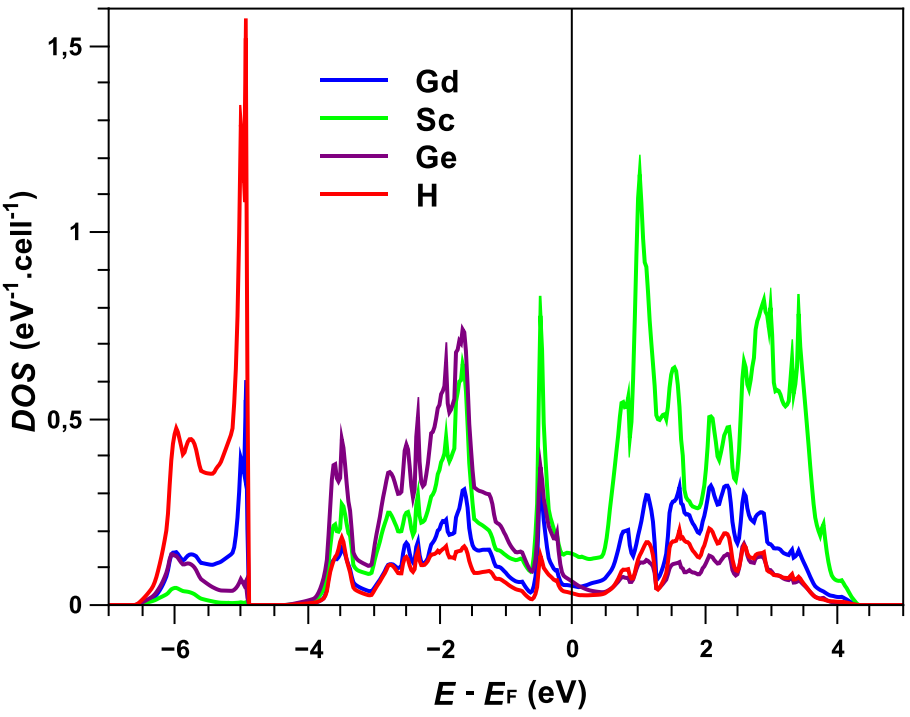

Figure 11. Partial densities of states (DOS) for the majority spin channel of GdScGeH, from DFT/HSE06 hybrid calculations. Due to the weak spin polarization, the partial DOS for majority and minority spin channels are very similar, except for filled and empty Gd 4f bands (that respectively lie around -8 and +4 eV with respect to Fermi level).

4. Conclusion

The hydrogenation of the intermetallic compound GdScGe has been investigated in order to induce physical properties modifications and understand the role of hydrogen insertion on them. Hydrogenation absorption curves and X-ray diffraction have shown that 1 atom of H f.u.$^{-1}$ is absorbed at 623 K and at a gas pressure between 0.5 and 4 MPa. DFT calculations also gave strong evidence that H atoms occupy the rare-earth tetrahedra [Gd_4] as interstitial sites. This absorption keeps the initial tetragonal space group *I*4/*mmm* but induces a strong elongation of the *c* parameter whereas *a* contracts slightly. As a consequence, the two types of layers within the structure are more compact and more separated, reducing the dimensionality of the crystal structure. More interestingly, hydrogenation almost destroys the ferromagnetic order observed in GdScGe below T_C= 350 K since GdScGeH undergoes a magnetic transition at 6 K only. The role of hydrogen insertion is thus drastic on the modifications of the magnetic properties and very different to what can be observed by chemical substitution in CeScSi-type compounds. For example, antimony substitution in GdScGe also leads to an increase of the *c*/*a* ratio (from 3.66 to 3.78) but this results in a structural transition from CeScSi- to CeFeSi-type structure.[25] This is not the case for GdScGe upon hydrogenation despite a stronger increase of the *c*/*a* ratio (from 3.66 to 3.97). In fact, the anisotropic volume change between GdScGe and its hydride is not the pertinent criteria to account for the vanishing of the ferromagnetic order. As demonstrated by DFT calculations, it is both the electron transfer from the conduction band to hydrogen and the chemical effect of Gd-H bonding which explains the loss of spin polarization after hydrogenation. Additionally, the appearance of the Gd-H bonding weakens the Gd-Sc interaction, whose role is essential to explain the high Curie temperature in GdScGe. Consequently, the induced polarization of the Sc-*d* state is strongly reduced as well as the magnetic coupling between Gd double layers through Sc orbitals. Another interesting effect is the resistivity change from a metallic to a non-metallic behavior upon hydrogenation. From DFT calculations we observe the opening of a pseudo-gap in the DOS at the Fermi level, together with a 2D electron density near E_F mainly distributed within the (*ab*) plane and very weakly along the *c*-axis. We suspect that the increase of resistivity at low temperature may be due to weak localization of electrons induced by structural defects or thermal activation of the conduction electrons. Finally, we can conclude that hydrogen insertion in GdScGe deeply reduces the dimensionality of both the magnetic coupling through the structure and the electron density distribution at the top of the valence band. This almost destroys the 3D magnetic order and contributes to reduce the metallic character of the pristine compound.

Supporting Information:

Additional characterizations on GdScGeH (sample 1) and additional table and figures from DFT calculations.

References

(1) Chevalier, B.; Tencé, S.; Gaudin, E.; Matar, S. F.; Bobet, J.-L. L. Various Magnetic Behaviors of the Hydrides Deriving from the Tetragonal CeFeSi-Type Compounds. *J. Alloys Compd.* **2009**, *480* (1), 43–45.

(2) Kamihara, Y.; Watanabe, T.; Hirano, M.; Hosono, H. Iron-Based Layered Superconductor $La(O_{1-x}F_x)FeAs$ (X = 0.05-0.12) with T_c = 26 K. *J. Am. Chem. Soc.* **2008**, *130* (11), 3296–3297.

(3) Zhao, J.; Huang, Q.; de la Cruz, C.; Li, S.; Lynn, J. W.; Chen, Y.; Green, M. A.; Chen, G. F.; Li, G.; Li, Z.; Luo, J. L.; Wang, N. L.; Dai, P. Structural and magnetic phase diagram of $CeFeAsO_{1-x}F_x$ and its relation to high-temperature superconductivity. *Nature Materials* **2008**, *7*(12), 953–959.

(4) Ren, Z. A.; Che, G.-C.; Dong, X.-L.; Yang, J.; Lu, W.; Yi, W.; Shen, X.-L.; Li, Z.-C.; Sun, L.-L.; Zhou, F.; et al. Superconductivity and Phase Diagram in Iron-Based Arsenic-Oxides $ReFeAsO_{1-\delta}$ (Re = Rare-Earth Metal) without Fluorine Doping. *EPL (Europhysics Lett.* **2008**, *83* (1), 17002.

(5) Chen, X. H.; Wu, T.; Wu, G.; Liu, R. H.; Chen, H.; Fang, D. F. Superconductivity at 43 K in $SmFeAsO_{1-x}Fx$. *Nature* **2008**, *453* (7196), 761–762.

(6) Chevalier, B.; Gaudin, E.; Tencé, S.; Malaman, B.; Fernandez, J. R.; André, G.; Coqblin, B. Hydrogenation Inducing Antiferromagnetism in the Heavy-Fermion Ternary Silicide CeRuSi. *Phys. Rev. B - Condens. Matter Mater. Phys.* **2008**, *77* (1), 1–10.

(7) Tencé, S.; André, G.; Gaudin, E.; Chevalier, B. Modulated Magnetic Structures of the Antiferromagnetic Hydride CeRuSiH. *J. Phys. Condens. Matter* **2008**, *20* (25), 255239.

(8) Tencé, S.; Matar, S. F.; André, G.; Gaudin, E.; Chevalier, B. Hydrogenation Inducing Ferromagnetism in the Ternary Antiferromagnet NdCoSi. *Inorg. Chem.* **2010**, *49* (11), 4836–4842.

(9) Tencé, S.; André, G.; Gaudin, E.; Bonville, P.; Al Alam, A. F.; Matar, S. F.; Hermes, W.; Pöttgen, R.; Chevalier, B. Huge Influence of Hydrogenation on the Magnetic Properties and Structures of the Ternary Silicide NdMnSi. *J. Appl. Phys.* **2009**, *106* (3), 33910.

(10) Bernardini, F.; Garbarino, G.; Sulpice, M.; Núñez-Regueiro; Gaudin, E.; Chevalier, B.; Méasson, M.-A.; Cano, A.; Tencé, S. Iron-Based Superconductivity Extended to the Novel Silicide LaFeSiH. *Phys. Rev. B* **2018**, *97*, 100504(R).

(11) Gaudin, E.; Matar, S. F.; Pöttgen, R.; Eul, M.; Chevalier, B. Drastic Change of the Ferromagnetic Properties of the Ternary Germanide GdTiGe through Hydrogen Insertion. *Inorg. Chem.* **2011**, *50* (21), 11046–11054.

(12) Singh, S. K.; Dhar, S. K.; Manfrinetti, P.; Palenzona, A.; Mazzone, D. High Magnetic

Transition Temperatures in RScT (R = Pr, Nd and Sm; T = Si and Ge) Compounds: Multiple Spin Reorientations in PrScGe. *J. Magn. Magn. Mater.* **2004**, *269* (1), 113–121.

(13) Singh, S. K.; Dhar, S. K.; Mitra, C.; Paulose, P. L.; Manfrinetti, P.; Palenzona, A. The Nature of Magnetism in CeScSi and CeScGe. *J. Phys. Condens. Matter* **2001**, *13* (16), 3753–3766.

(14) Manfrinetti, P.; Pani, M.; Palenzona, A.; Dhar, S. K.; Singh, S. K. Single Crystal Study of the High-Curie-Temperature Ferromagnet $Gd_{1.02}Sc_{0.98}Ge$ and of $Gd_{2.38}Sc_{2.62}Ge_3$. *J. Alloys Compd.* **2002**, *334* (1–2), 9–13.

(15) Couillaud, S.; Gaudin, E.; Franco, V.; Conde, A.; Pöttgen, R.; Heying, B.; Rodewald, U. C.; Chevalier, B. The Magnetocaloric Properties of GdScSi and GdScGe. *Intermetallics* **2011**, *19* (10), 1573–1578.

(16) Nikitin, S. A.; Ovtchenkova, I. A. A.; Skourski, Y. V. V.; Morozkin, A. V. Magnetic Properties of Ternary Scandium Rare Earth Silicides and Germanides. *J. Alloys Compd.* **2002**, *345* (1–2), 50–53.

(17) Manfrinetti, P.; Morozkin, A. V.; Isnard, O.; Henry, P.; Palenzona, A. Magnetic Structure of the CeScSi-Type RScGe Compounds (R = Pr, Nd, Tb). *J. Alloys Compd.* **2008**, *450* (1–2), 86–91.

(18) Tencé, S.; Isnard, O.; Gaudin, E.; Chevalier, B. Synthesis and Magnetic Properties of the Ternary Germanide TbScGe. *J. Alloys Compd.* **2013**, *560*, 195–199.

(19) Mishra, S. N. Magnetic Interactions in Equi-Atomic Rare-Earth Intermetallic Alloys RScGe (R = Ce, Pr, Nd and Gd) Studied by Time Differential Perturbed Angular Correlation Spectroscopy and Ab Initio Calculations. *J. Phys. Condens. Matter* **2009**, *21* (11), 115601.

(20) Skorek, G.; Deniszczyk, J.; Szade, J.; Tyszka, B. Electronic Structure and Magnetism of Ferromagnetic GdTiSi and GdTiGe. *J. Phys. Condens. Matter* **2001**, *13* (29), 6397.

(21) Tencé, S.; Mahon, T.; Gaudin, E.; Chevalier, B.; Bobet, J.-L. J.-L.; Flacau, R.; Heying, B.; Rodewald, U. C.; Pöttgen, R. Hydrogenation Studies on NdScSi and NdScGe. *J. Solid State Chem.* **2016**, *242*, 168–174.

(22) Chevalier, B.; Hermes, W.; Heying, B.; Rodewald, U. C.; Hammerschmidt, A.; Matar, S. F.; Gaudin, E.; Pöttgen, R. New Hydrides REScSiH and REScGeH (RE = La, Ce): Structure, Magnetism, and Chemical Bonding. *Chem. Mater.* **2010**, *22* (17), 5013–5021.

(23) Nuss, J.; Wedig, U.; Jansen, M. Geometric Variations and Electron Localizations in Intermetallics: The Case of La_2Sb Type Compounds. *Zeitschrift fur Anorg. und Allg. Chemie* **2011**, *637* (13), 1975–1981.

(24) Wu, J.; Gong, Y.; Inoshita, T.; Fredrickson, D. C.; Wang, J.; Lu, Y.; Kitano, M.; Hosono, H. Tiered Electron Anions in Multiple Voids of LaScSi and Their Applications to Ammonia Synthesis. *Adv. Mater.* **2017**, *1700924*, 1–7.

(25) Guillou, F.; Pathak, A. K.; Hackett, T. A.; Paudyal, D.; Mudryk, Y.; Pecharsky, V. K. Crystal, Magnetic, Calorimetric and Electronic Structure Investigation of $GdScGe_{1-x}Sb_x$ Compounds. *J. Phys. Condens. Matter* **2017**, *29* (48), 485802.

(26) Liu, X.; Matsuishi, S.; Fujitsu, S.; Ishigaki, T.; Kamiyama, T.; Hosono, H. Layered Hydride CaNiGeH with a ZrCuSiAs-Type Structure: Crystal Structure, Chemical

Bonding, and Magnetism Induced by Mn Doping. *J. Am. Chem. Soc.* **2012**, *134* (28), 11687–11694.

(27) Bobet, J.-L.; Pechev, S.; Chevalier, B.; Darriet, B. Structural and Hydrogen Sorption Studies of $NdNi_{5-x}Al_x$ and $GdNi_{5-x}Al_x$. *J. Alloys Compd.* **1998**, *267* (1–2), 136–141.

(28) Petříček, V.; Dušek, M.; Palatinus, L. Crystallographic Computing System JANA2006: General Features. *Zeitschrift für Krist. - Cryst. Mater.* **2014**, *229* (5).

(29) Dufek, V.; Petrů, F.; Brožek, V. Über Sauerstoff-Haltige Verbindungen Vom Strukturtyp B1 Der Ersten Vier Übergangsmetalle. *Monatshefte für Chemie* **1967**, *98* (6), 2424–2430.

(30) Kresse, G.; Hafner, J. Ab Initio Molecular Dynamics for Liquid Metals. *Phys. Rev.* **1993**, *47* (1), 558–561.

(31) Kresse, G.; Furthmüller, J. Efficiency of Ab Initio Total Energy Calculations for Metals and Semiconductors Using a Plane Wave Basis Set. *Comput. Mat. Sci.* **1996**, *6* (1), 15.

(32) Blöchl, P. E. Projector Augmented-Wave Method. *Phys. Rev. B* **1994**, *50* (24).

(33) Perdew, J. P., Burke, K. & Ernzerhof, M. Generalized Gradient Approximation Made Simple. *Phys. Rev. Lett.* **1996**, *77* (3), 3865–3868.

(34) Dudarev, S. L.; Botton, G. A.; Savrasov, S. Y.; Humphreys C. J.; Sutton, A. P. Electron-energy-loss spectra and the structural stability of nickel oxide: an LSDA+U study. *Phys. Rev. B* **1998**, 57, 1505.

(35) Heyd, J.; Scuseria, G. E.; Ernzerhof, M. Hybrid Functionals Based on a Screened Coulomb Potential. *J. Chem. Phys.* **2003**, *118* (18), 8207–8215.

(36) Krukau, A. V.; Vydrov, O. A.; Izmaylov, A. F.; Scuseria, G. E. Influence of the Exchange Screening Parameter on the Performance of Screened Hybrid Functionals. *J. Chem. Phys.* **2006**, *125* (22).

(37) Oelerich, W.; Klassen, T.; Bormann, R. Metal Oxides as Catalysts for Improved Hydrogen Sorption in Nanocrystalline Mg-based Materials. *J. Alloys Compd.* **2001**, *315*, 237–242.

(38) Ellner, M.; Reule, H.; Mittemeijer, E. J. Unit Cell Parameters and Densities of the Gadolinium Dihydride GdH_2. *J. Alloys Compd* **1998**, *279*, 179–183.

(39) Ganapathy, E. V.; Kugimiya, K.; Steinfink, H.; Tchernev, D. I. Magnetic Properties of Some Rare Earth Silicides: GdSi, Gd_5Si_3, $Dy_{5-x}Nd_xSi_3$. *Journal of The Less-Common Metals*. 1976, pp 245–258.

(40) Ritter, C.; Dhar, S. K.; Kulkarni, R.; Provino, A.; Paudyal, D.; Manfrinetti, P.; Gschneidner, Jr., K. A. Electronically- and Crystal-Structure-Driven Magnetic Structures and Physical Properties of RScSb (R = Rare Earth) Compounds: A Neutron Diffraction, Magnetization and Heat Capacity Study. *J. Phys. Condens. Matter* **2014**, *26* (36), 366001.

(41) Lemoine, P.; Vernière, A.; Venturini, G.; Marêché, J. F.; Capelli, S.; Malaman, B. Magnetic Properties and Magnetic Structures of the CeScSi-Type RMgPb (R=Ce-Nd, Sm, Gd-Tm) Compounds. *J. Magn. Magn. Mater.* **2012**, *324* (19), 2937–2952.

(42) Tencé, S.; Heying, B.; Janka, O.; Pöttgen, R.; Chevalier, B. Hydrogenation-Induced Cerium Valence Change in CeNiZn. *J. Alloys Compd.* **2017**, *724*, 515–519.

(43) Nikitin, S. A.; Tristan, N. V.; Palewski, T.; Skourski, Y. V.; Nenkov, K.; Verbetsky, V. N.; Salamova, A. A. Metal-Semiconductor-Insulator Transitions in R3Ni Compounds Induced by Hydrogenation. *J. Alloys Compd.* **2001**, *314* (1–2), 22–28.

(44) Liu, X. B.; Altounian, Z.; Han, Xianghua; Poudyal, Narayan; Liu, J. Ping. Magnetic state and exchange interaction in GdScGe: ab initio study. *J. Applied Phys.* **2013**, 113, 17E103.

Table of Content (TOC)

Hydrogen atoms have been inserted in the intermetallic compound GdScGe to synthesize the hydride GdScGeH. It results in a spectacular vanishing of the 3D ferromagnetic order as well as a change of conductivity from metallic to non-metallic behavior.